



# A model for intracellular actin waves explored by nonlinear local perturbation analysis <sup>☆</sup>



May Anne Mata <sup>a,b</sup>, Meghan Dutot <sup>a</sup>, Leah Edelstein-Keshet <sup>a</sup>, William R. Holmes <sup>c,\*</sup>,<sup>1</sup>

<sup>a</sup> Department of Mathematics, University of British Columbia, Vancouver, BC, V6T 1Z2, Canada

<sup>b</sup> Department of Math, Physics, and Computer Science, University of the Philippines Mindanao, Davao City, Philippines

<sup>c</sup> Department of Mathematics, University of California, Irvine, CA 92697, United States

## HIGHLIGHTS

- We propose a model for F-actin interacting with its nucleation promoting factors.
- The model consists of 3 PDES of the reaction-diffusion type.
- The model exhibits novel dynamics of waves and propagating patterns.
- A non-linear, local perturbation analysis is used to investigate pattern initiation.
- Our model depicts the minimal set of interactions that can produce these dynamics.

## ARTICLE INFO

### Article history:

Received 22 February 2013

Received in revised form

7 June 2013

Accepted 18 June 2013

Available online 2 July 2013

### Keywords:

Actin waves

Nucleation promoting factors

Reaction diffusion systems

Pattern formation

Nonlinear stability analysis

## ABSTRACT

Waves and dynamic patterns in chemical and physical systems have long interested experimentalists and theoreticians alike. Here we investigate a recent example within the context of cell biology, where waves of actin (a major component of the cytoskeleton) and its regulators (nucleation promoting factors, NPFs) are observed experimentally. We describe and analyze a minimal reaction diffusion model depicting the feedback between signalling proteins and filamentous actin (F-actin). Using numerical simulation, we show that this model displays a rich variety of patterning regimes. A relatively recent nonlinear stability method, the Local Perturbation Analysis (LPA), is used to map the parameter space of this model and explain the genesis of patterns in various linear and nonlinear patterning regimes. We compare our model for actin waves to others in the literature, and focus on transitions between static polarization, transient waves, periodic wave trains, and reflecting waves. We show, using LPA, that the spatially distributed model gives rise to dynamics that are absent in the kinetics alone. Finally, we show that the width and speed of the waves depend counter-intuitively on parameters such as rates of NPF activation, negative feedback, and the F-actin time scale.

Published by Elsevier Ltd.

## 1. Introduction

The actin cytoskeleton is an important determinant of cell shape, function, and motility. Hence, the dynamics and assembly of filamentous actin (F-actin) from its subunits (G-actin) is highly regulated in living cells. Recent experimental observations have shown remarkable spontaneously generated spatio-temporal patterns of F-actin in cells such as *Dictyostelium discoideum* (Vicker, 2002a, 2002b), neutrophils (Weiner et al., 2007), fibroblasts (Millius et al., 2009) and mast cells (Wu et al., 2013). The patterns include

stationary fronts, moving spots, and moving waves, providing a rich set of “benchmark dynamics” that models for actin organization should address. An interesting theoretical question is what minimal, biologically grounded mechanism suffices to explain such waves and patterns.

Actin interacts with other proteins that regulate its nucleation and assembly. Experimental data supports the role of these regulatory proteins (often denoted actin “nucleation promoting factors,” abbreviated NPFs) in producing the dynamic patterns of actin (Bretschneider et al., 2004, 2009; Gerisch et al., 2004; Xiong et al., 2010). Such observations have led to physical and biophysical models that aim to understand the interactions between these signalling proteins and actin (Weiner et al., 2007; Dubrovinski and Kruse, 2008; Whitlam et al., 2009; Iglesias and Devreotes, 2012). However little effort so far has been devoted to using mathematical methods to investigate these phenomena, motivating our exploration in this paper.

<sup>☆</sup>Funded by NSERC discovery grant to LEK and by NIH R01 GM086882 to Anders Carlsson and LEK.

\* Corresponding author. Tel.: +1 949 824 3217; fax: +1 949 824 7993.

E-mail address: [wrrholmes@uci.edu](mailto:wrrholmes@uci.edu) (W.R. Holmes).

<sup>1</sup> WRH conceived, designed, and supervised this work.

In a previous paper (Holmes et al., 2012a), we considered signalling proteins such as small GTPases (Rac, Rho, and Cdc42) as putative NPFs. Upstream of actin, small GTPases have been observed to undergo spontaneous symmetry breaking leading to wave dynamics. Polarization of Rac was shown to be required for formation of Hem1/F-actin waves in Weiner et al. (2007). Machacek et al. (2009) provided quantitative evidence for the correlation of Cdc42, Rac1, and RhoA wave dynamics with F-actin mediated edge protrusion. In Wu et al. (2013), waves of Cdc42 were shown to be correlated in both space and time with waves of F-actin.

We describe the interactions of F-actin and its regulators by a system of reaction-diffusion equations (RDEs) and view the formation of waves and other dynamics as a pattern formation process. More broadly, reaction-diffusion models have been used to investigate pattern formation in physical or physico-chemical processes (Cross and Hohenberg, 1993; Maini et al., 1997; Gollub and Langer, 1999), morphogenesis and development (Turing, 1952; Murray, 1981), or distributions of populations in a changing environment (Segel and Jackson, 1972; Okubo and Levin, 2002; Cantrell and Cosner, 2004; Yizhaq et al., 2005). A common sufficient (and usually necessary) condition for patterning in these cases is different rates of diffusion. The system discussed here, like many biochemical regulatory systems, is characterized by not just different, but vastly different rates of diffusion, which we exploit to simplify model analysis.

To search the parameter space of this model and investigate the structure responsible for initiation of patterning in different regimes of behavior, we utilize a relatively new nonlinear stability analysis method for such systems, the *Local Perturbation Analysis* (LPA) (Walther et al., 2012). This method takes advantage of the disparity between slow and fast diffusion timescales to reduce the system of RDE's to a system of ODE's whose linear and nonlinear stability properties mimic those of the RDE's. Results of this analysis in conjunction with linear stability analysis and numerical simulation demonstrate a rich collection of patterning behaviors distinct from those observed in other systems. We identify the mathematical structure responsible for these distinct dynamics and show that this is a minimal model capable of producing such dynamics.

In our previous paper (Holmes et al., 2012a), we presented preliminary analysis of the actin wave model, together with some simulation results. In this follow-up paper we have two distinct aims. (1) To understand the regimes of behavior of the waves in greater detail and to characterize parameter dependence of wave attributes such as speed and width. (2) To highlight and explain features of LPA and its mathematical properties. Our detailed (though informal) exposition is meant to enable the reader to use similar methods on related problems.

## 2. Biological and modeling background

Many previous models of actin waves (Weiner et al., 2007; Doubrovinski and Kruse, 2008; Whitlam et al., 2009; Carlsson, 2010a; Doubrovinski and Kruse, 2011; Iglesias and Devreotes, 2012), reviewed in Carlsson (2010b) and Holmes et al. (2012a), are based on F-actin interacting with nucleation promoting factors such as Hem1 Weiner et al. (2007) and WASP or Scar/Wave (Bretschneider et al., 2004, 2009; Gerisch et al., 2004; Xiong et al., 2010). Some of these models consider the length or angular distributions of F-actin, and some depict the interactions of individual actin filaments (Carlsson, 2010a).

In contrast, we consider a simplified model that can be analyzed mathematically. We focus on signalling proteins (small GTPases), coupled to a minimal F-actin representation. Our motivation for so

doing is as follows: (a) small GTPases (such as Cdc42 and Rac) are known to regulate the assembly of F-actin (Machacek et al., 2009; Mackay and Hall, 1998; Ridley, 2006; Hall, 1998; Sit and Manser, 2011) and participate in the propagation of actin waves (Weiner et al., 2007; Machacek et al., 2009; Wu et al., 2013). (b) A minimal model of small GTPases (Mori et al., 2008, 2011) exhibits wave-based symmetry-breaking and formation of a simple polarization pattern. (c) There is evidence for the existence of feedback between F-actin and the small GTPases; see experimental work in Xu et al. (2003), Sasaki et al. (2004), Sasaki et al. (2007) on the PI3K pathway and Calderwood et al. (2000), Abram and Lowell (2009) on integrins. (d) Combining the minimal GTPase model with a simplified F-actin model leads to a range of interesting patterns, as we have already described in Holmes et al. (2012a). As we sought a model of sufficient simplicity to yield mathematical insights, this minimal model proved to be ideal.

Briefly, small GTPases are proteins that cycle between an active state  $A$  (bound to the cell membrane) and an inactive state  $I$  (in the cytosol, the fluid cell interior). GTPases are activated by GEFs and inactivated by GAPs. In the previous work, we investigated the role of these proteins in cell polarization, arriving at a simple caricature in Mori et al. (2008) that was analyzed mathematically in Mori et al. (2011). We showed that the  $A, I$  model sustains waves that decelerate and stop inside the cell domain; this behavior was termed “wave-pinning”. Here we ask whether a small extension of the  $A, I$  model to include feedback to and from F-actin would engender any patterns similar to those observed experimentally. As we show in this paper, this proves to be the case.

### 2.1. The regulatory sub-model and its “wave-pinning” behavior

In this section, we briefly describe the regulatory sub-model. Let  $A, I$  represent active and inactive forms of a small GTPase protein with  $A$  bound to the membrane and  $I$  freely diffusing in the cell interior. This  $A, I$  system plays a regulatory role for F-actin assembly (analogous to the role of nucleation promoting factors, abbreviated NPFs) as well as being affected by feedback from F-actin. Equations for  $A, I$ , modified slightly from Mori et al. (2008), are

$$\frac{\partial A}{\partial t} = f(A, I) + \tilde{D}_A \Delta A, \quad \frac{\partial I}{\partial t} = -f(A, I) + \tilde{D}_I \Delta I \quad (1a)$$

$$f(A, I) = \tilde{\delta} \left[ \left( k_0 + \gamma \frac{A^n}{\tilde{A}_0^n + A^n} \right) I - A \right]. \quad (1b)$$

with  $\tilde{D}_A < \tilde{D}_I$  and no flux boundary conditions. Note that we used  $A, I$  here to denote the amount of active and inactive NPFs. In the interconversion of  $A$  and  $I$  (which corresponds to activation and inactivation), the total amount  $A+I$  is conserved and  $A$  enhances its own activation. This positive feedback is represented by a Hill function (with magnitude  $\gamma$ , sharpness controlled by  $n \geq 2$ , and  $\tilde{A}_0$  the typical level of  $A$  at which positive feedback “turns on”). The parameter  $k_0$  is the basal rate of activation and  $\tilde{\delta}$  sets the overall rate of dynamics. Details for the choice of this function are motivated in Marée et al. (2006), Jilkin et al. (2007), Dawes and Edelstein-Keshet (2007), and Mori et al. (2008) based on known and hypothesized properties of the small GTPases.

In Holmes et al. (2012b), we noted two regimes of behavior. In one regime, arbitrarily small noise can destabilize a homogeneous steady state (HSS) and lead to patterning, as in classical Turing pattern formation. In the second regime, the HSS is linearly stable, and only a sufficiently large perturbation can lead to patterning. This perturbation produces a region of high activity that spreads then stalls (“wave-pinning”). The properties of this model responsible for wave-pinning include (1)  $\tilde{D}_A < \tilde{D}_I$  (resulting from membrane bound versus free diffusing character), and

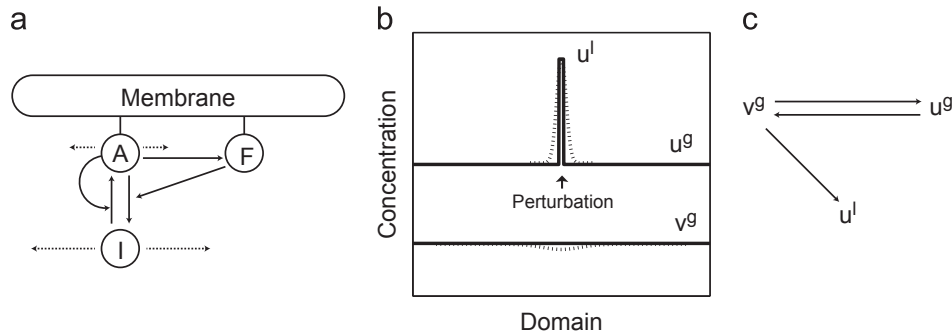


**Fig. 1.** (a) A schematic diagram of interactions between F-actin ( $F$ ) and its regulatory proteins (NPFs).  $A$  is active, membrane-bound protein and  $I$  is its inactive cytosolic form. We assume that  $A$  promotes actin nucleation and assembly. We also assume positive feedback from  $A$  and negative feedback from  $F$  to the rate activation of  $A$ . Total  $A + I$  is conserved. Dashed arrow represent slow or fast diffusion (not to scale). (b) A spatially localized perturbation showing the idealization that leads to the LPA system of local and global variables (solid), and the actual behavior in the full RD system (dotted). (c) Schematic representation of interactions of the local and global LPA variables.  $u_g$ ,  $v_g$  interact exactly as in the well-mixed system.  $u_l$  is local, and influenced by (but does not affect) the global variables.

(2) conservation of the total  $A+I$  in the domain. Heuristically, auto-activation of  $A$  induces a region of locally high activity. Diffusion causes this region to spread. Depletion of  $I$  as the wave spreads causes the wave to slow and stall in the interior of the domain.

### 3. Model for the full system: regulators and F-actin with positive and negative feedback

We asked whether linking the  $A, I$  signalling model to an F-actin equation could account for some of the dynamic F-actin patterns and waves. In experimentally observed actin waves, it is seen that a localized wave of actin nucleators leads and a localized F-actin wave follows Weiner et al. (2007). This observation suggests negative feedback from F-actin to NPFs. These ideas led us to adopt a framework similar to the FitzHugh Nagumo model, with nonlinear wave generation coupled to slow feedback as depicted in Fig. 1(a). We investigate how this coupling leads to both stationary and wave dynamics.

The model, schematically outlined in Fig. 1(a), represents the interactions of the active ( $A$ ) and inactive ( $I$ ) regulatory protein (NPF) with F-actin ( $F$ ). The equations of the full model (after nondimensionalization, see Appendix B) are

$$\frac{\partial A}{\partial t} = f(A, I, F) + D_A \Delta A, \quad \frac{\partial I}{\partial t} = -f(A, I, F) + D_I \Delta I, \quad (2a)$$

$$\frac{\partial F}{\partial t} = \epsilon h(A, F), \quad \text{where } h(A, F) = k_n A - k_s F, \quad (2b)$$

$$f(A, I, F) = \left( k_0 + \gamma \frac{A^3}{A_0^3 + A^3} \right) I - \left( s_1 + s_2 \frac{F}{1+F} \right) A. \quad (2c)$$

We refer to this as the full model or as the F-actin regulation model. Neumann boundary conditions are assumed for  $A, I$ . The regulatory kinetics  $f$  are as in (1), with the modification that F-actin exerts a net negative feedback on its own regulators. Here we have chosen to depict this feedback with a Michaelis–Menten actin-dependent rate of inactivation of  $A$ . This saturating response prevents over-damping of the entire system. The parameters  $s_1$  and  $s_2$  represent the relative contributions of basal inactivation, and inactivation due to feedback from  $F$ .

We are particularly interested in understanding how the balance between NPF activation and actin-feedback mediated inactivation affect wave formation and propagation. We thus focus on the parameters  $k_0$  and  $s_2$  that affect this balance. Other combinations of (in)activation parameters yield similar results. That is, an analysis of the parameter space structure with respect to  $\gamma$  and  $s_2$ , for example, is qualitatively the same. The parameter  $\epsilon$

determines the relative timescales of actin and regulatory protein dynamics, respectively, and will be considered as well. We assume that the F-actin feedback occurs on a slower timescale, so that  $\epsilon < 1$ . In models for wave propagation in neurons, variables that play a similar role to  $F$  are often denoted “slow”, or “recovery” or “refractory”. We will use similar terminology here. The balance between feedback and activation, and the effect of relative timescales will be investigated in subsequent sections.

We have made a few standard simplifying assumptions in formulating the model. We assume that the cell has spread onto a flat surface and that its depth is uniformly thin. To leading order, the concentration of  $I$  in the cell interior is then uniform in the depth direction. We further neglect structures such as the nucleus and consider a 1D strip of uniform width along the diameter of the cell.  $A, I, F$  are then functions of a single spatial variable ( $x$ ) and time. The membrane bound/freely diffusing proteins differ only in their rates of diffusion, avoiding the issue of multiple physical compartments. See Holmes et al. (2012a, 2012b) for details and justification. It is easily seen that  $A, I$  in Eq. (2) satisfy a conservation law  $\int_0^1 (A(x, t) + I(x, t)) dx = T_{NPF} = 1$ .

### 4. Methods

Here we define terminology and introduce the techniques used to analyze the model. Consider a system of reaction-diffusion equations

$$\frac{\partial u}{\partial t} = f(u, v; p) + D_u \frac{\partial^2 u}{\partial x^2}, \quad (3a)$$

$$\frac{\partial v}{\partial t} = g(u, v; p) + D_v \frac{\partial^2 v}{\partial x^2}, \quad (3b)$$

that has been nondimensionalized appropriately, so that  $f, g = O(1)$  with no flux boundary conditions on  $[-1, 1]$ . Here,  $p$  represents a vector of system parameters and in general,  $u, v$  could be vector valued with  $D_u$  and  $D_v$  being diagonal matrices encoding diffusion coefficients. We further restrict attention to a class of RDEs involving fast and slow diffusing variables so that  $D_u < 1 < D_v$ . For example,  $u = (A, F)$  represents membrane bound or stationary proteins and  $v = (I)$  represents cytosolic proteins. We also frequently refer to the “well-mixed”, i.e. spatially homogeneous variant of this system:

$$\frac{du}{dt} = f(u, v; p), \quad \frac{dv}{dt} = g(u, v; p). \quad (4)$$

The Local Perturbation Analysis (LPA) is an effective method for analyzing fast/slow systems of the form (3) (Walther et al., 2012). This method was introduced in the Grieneisen PhD thesis (2009) and has

been used extensively in Marée et al. (2006, 2012), Holmes et al. (2012b, 2012a), to parameterize and explore models of signalling networks.

LPA is an approximation of the dynamics of a pulse under the limit where  $D_u \rightarrow 0$  ( $u$  is infinitely slow diffusing) and  $D_v \rightarrow \infty$  ( $v$  is infinitely fast diffusing, reminiscent of a “shadow system” (Nishiura, 1982)). Let  $u^l(t)$  denote the amplitude of a spatially localized perturbation and  $u^g(t)$ ,  $v^g(t)$  the essentially homogeneous background levels of  $u$ ,  $v$ . Then  $u^l$  will grow or decay independently of  $u^g$ . Inhomogeneities of  $v$  will be instantly smoothed out, leaving only a global quantity  $v^g$ . Assuming a perturbation with negligible total mass (i.e. whose “area” vanishes with  $D_u$ ),  $v^g$  will be affected only by  $u^g$  (see Fig. 1(c)). Under this limiting approximation, the dynamics of the narrow pulse-like perturbation can be approximated by ODEs for  $(u^l(t), u^g(t), v^g(t))$ :

$$\frac{du^g}{dt}(t) = f(u^g, v^g; p), \quad (5a)$$

$$\frac{dv^g}{dt}(t) = g(u^g, v^g; p), \quad (5b)$$

$$\frac{du^l}{dt}(t) = f(u^l, v^g; p). \quad (5c)$$

We refer to this system as the LPA-ODE's, and to the analysis of its behavior as the Local Perturbation Analysis (LPA).

Before applying this method to the actin–regulatory model, we collect a few results about LPA and the type of information it is capable of providing. Details of the reasoning and validation of a number of results are provided in the Appendix.

Let  $(u^s, v^s)$  denote the homogeneous steady state of (3). Then  $(u^g, v^g, u^l) = (u^s, v^s, u^s)$  is a fixed point of the LPA-ODE's (5). Thus stability of the HSS to a localized perturbation (LPA stability) is determined by eigenvalues of

$$J_{LP} = \begin{bmatrix} f_u(u^s, v^s; p) & f_v(u^s, v^s; p) & 0 \\ g_u(u^s, v^s; p) & g_v(u^s, v^s; p) & 0 \\ 0 & f_v(u^s, v^s; p) & f_u(u^s, v^s; p) \end{bmatrix}. \quad (6)$$

In the Appendix we provide arguments to support the following properties.

Property 1: LPA recapitulates linear stability results for the well-mixed system (4); that is to say, eigenvalues of the linearized well-mixed system about  $(u^s, v^s)$  are contained in the spectrum of (6). These will be referred to as the well-mixed eigenvalues of  $J_{LP}$ .

Property 2: LPA recapitulates linear stability results for the full reaction-diffusion system (Turing stability analysis). More precisely, the remaining eigenvalues of  $J_{LP}$  approximate Turing eigenvalues obtained by linearizing the full system of RDE's about  $(u^s, v^s)$ . We will refer to these as the “local” eigenvalues of  $\{\lambda_j^{LP}\}$ .

In Appendix A, we show Property 2 in a  $2 \times 2$  system. In the  $3 \times 3$  ( $A, I, F$ ) system, we show this property numerically. In higher order systems, we conjecture (but do not prove) that the same property holds.

The advantages of the LPA method are as follows:

- LPA mirrors predictions of other stability analysis methods; it detects the number, values, and stability of spatially homogeneous steady states (HSS).
- LPA predicts the response of the system to large amplitude perturbations. This property will be illustrated by example.
- Since LPA leads to a set of ODE's (5) and harnesses standard bifurcation techniques and software, it is substantially simpler to implement than other nonlinear, weakly nonlinear (Rubinstein et al., 2012), or asymptotic methods (Iron and Ward, 2000).

**Table 1**

Default nondimensional parameter values used in simulations of the full model. These values produce a reflecting pulse. Bracketed values produce a wave train. The abbreviation NPF represents the regulatory protein. Values for most dimension-carrying NPF parameters are based on small GTPases in Mori et al. (2008), and lead approximately to the above dimensionless values based on scaling discussed in Appendix B.

| Parameter  | Value      | Description  |
|------------|------------|--|
| $D_A$      | 0.00033    | Diffusion coefficient of $A$                       |
| $D_I$      | 0.033      | Diffusion coefficient of $I$                       |
| $k_0$      | 0.05 (0.2) | Basal rate of activation of NPF                    |
| $\gamma$   | 1          | Magnitude of NPF positive feedback                 |
| $A_0$      | 0.4        | Level of active NPF for positive feedback to occur |
| $s_1$      | 0.5        | Basal NPF inactivation rate                        |
| $s_2$      | 0.6 (1.2)  | F-actin-mediated NPF inactivation rate             |
| $k_n$      | 2.0        | Rate of F-actin nucleation by NPF                  |
| $k_s$      | 0.25       | F-actin disassembly rate                           |
| $\epsilon$ | 0.1        | F-actin dynamics rate parameter                    |
| $T_{NPF}$  | 1          | Total amount of NPF                                |

Further, LPA is scalable to systems with many interacting components provided their components are separable into fast and slow diffusion classes. (Within a class, diffusivities need not be the same.) While this scalability will not be illustrated here (given the relatively few components of the actin waves model), we refer the reader to Holmes et al. (2012b) for an example of a complex system with many interacting components to which this method was successfully applied.

While LPA makes useful predictions under specific conditions, it also has limitations as follows:

- LPA applies only to RDEs with fast-slow variables, and not to reaction-advection PDEs.
- LPA does not approximate the full dynamics of RDEs nor the evolution of their solutions, only stability properties.
- The LPA approximation breaks down if the perturbation becomes very large or spreads in space. (This leads to interactions between local and global variables and boundary layer issues).
- LPA provides no information about wave numbers of destabilizing periodic perturbations (predicted by Turing analysis), since spatial scales are absent in the asymptotic limit.

With these caveats in mind, we next apply LPA to the actin waves model.

## 5. Analysis of the ( $A, I, F$ ) model

Parameter values for the underlying  $A, I$  dynamics are based on Mori et al. (2008). In absence of conclusive experimental data, feedback from F-actin is chosen to be in a range that is neither too strong nor too weak. All parameters are nondimensionalized as discussed in Appendix B and listed in Table 1.

We apply the local perturbation reduction to (2) and analyze the resulting LPA-ODE's to determine regimes of pattern initiation. We focus on how the basal activation rate ( $k_0$ ) and the negative feedback from F-actin ( $s_2$ ) influence dynamics. (Other parameters were tested and found to produce similar results. For example, the behavior relative to  $s_1$  is reciprocal to that relative to  $k_0$ . Results for  $\gamma$  were similar, and are omitted for brevity.) After the LPA, we explore the long-term dynamics of the patterns with full RDE simulations. See Appendix D for details about numerical implementation.

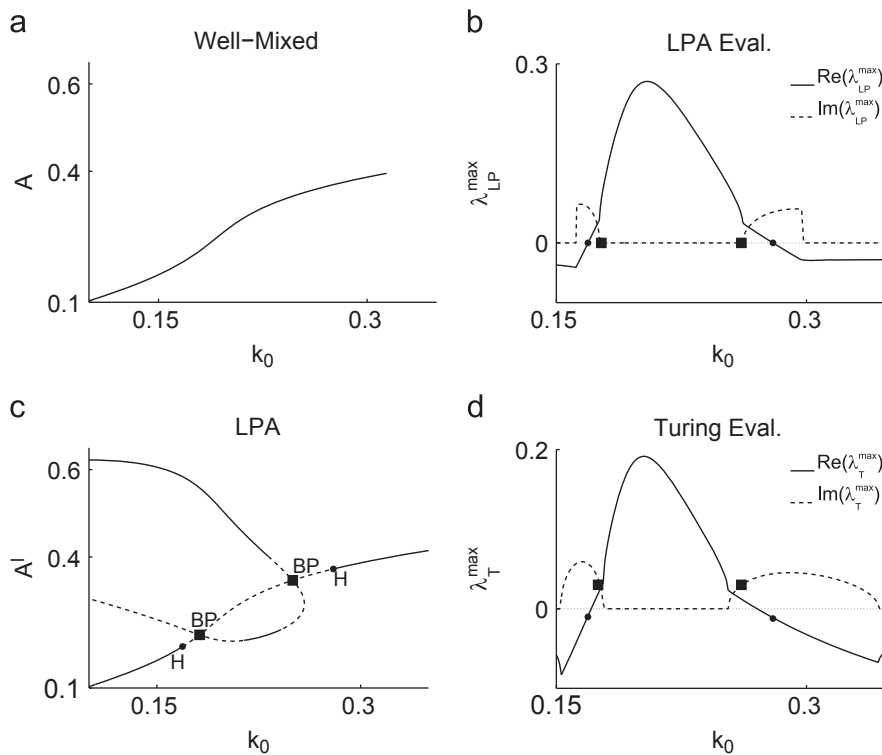


**Fig. 2.** Bifurcation analysis and eigenvalues in the actin-wave model for  $s_1 = 0.7$ ,  $s_2 = 0.7$ ,  $\tilde{\epsilon} = 0.1$  and other parameters at default values. *Left panels:* analysis of well-mixed (a) and LPA (c) ODE's plotting steady states of  $A$  and  $A^l$  respectively versus the basal activation rate  $k_0$  (solid=stable, dashed=unstable). The well-mixed model has a single stable steady state (a). The LPA system (c) has the same global branch, and additional local branches.  $\blacksquare$ , BP=branch points,  $\bullet$ , H=Hopf bifurcation. *Right panels:* A comparison of maximal (with largest real parts) LPA (b) and Turing (d) eigenvalues versus  $k_0$  (solid=real, dashed=imaginary parts). Symbols  $\blacksquare$ ,  $\bullet$ , mark the corresponding  $k_0$  values in (c). Hopf points correspond to zero real part and branch points to zero imaginary parts of  $\lambda_{LP}^{\max}$ . The eigenvalues in (b) and (d) are similar and the Hopf and B bifurcations closely relate to bifurcations of the RDE model.

### 5.1. The well-mixed system

A standard bifurcation analysis of the well-mixed variant of the system (2) with respect to  $k_0$  leads to Fig. 2(a), where we display the steady state  $A$ . There is a single unique HSS that is stable for all  $k_0$  values, given the default parameter set.

### 5.2. Local perturbation analysis (LPA)

We set up LPA equations for the full actin–regulatory protein model (see Eq. (C.1)). In doing so, we treat the non-diffusive F-actin and the active protein  $A$  as slow variables and inactive protein  $I$  (rapidly diffusing in the cytosol) as a fast variable. Consequently, the LPA equations have variables  $A^g$ ,  $I^g$ ,  $F^g$ ,  $A^l$ ,  $F^l$ .

A bifurcation analysis of the LPA equations (C.1) is shown for  $A^l$  versus  $k_0$  in Fig. 2(c). Comparing this diagram to the diagram in Fig. 2(a), the monotonically increasing well-mixed branch (hereafter denoted the “global branch”) appears in both as expected. We also find new features in the LPA diagram, including a second “local branch” emanating from branch points (BP). This local branch represents additional states that only the local variables can attain.

Interpreting the LPA bifurcation diagram of Fig. 2(c) from left to right, we first find that for small  $k_0$ , the global branch is stable to small perturbations, whereas the local branch has both unstable (dashed) and stable (solid) regions. Taken together, the global and local branches demonstrate a response threshold: a local perturbation large enough to elevate  $A^l$  above the (dashed) threshold will be attracted to the upper (stable) local branch while the global variables remain at their unique fixed point (lowest, global branch). Significantly, as the background rate of activation of regulatory protein increases, the size of the

stimulating pulse needed to produce a patterned response decreases. This result implies that the system becomes more sensitive to stimulation.

In the LPA diagram, we also find Hopf bifurcations (H) at which the global branch loses stability. Here, the three “well-mixed” eigenvalues have negative real parts (indicating stability). Thus the instability must arise from the two remaining “local” eigenvalues, in this case complex conjugates whose real and imaginary parts plotted in Fig. 2(b). At H, these eigenvalues cross the imaginary axis. This fact indicates that oscillations arise not from the kinetics of the well-mixed system (where no interesting bifurcations take place) but rather from the interactions of the local variables  $A^l$ ,  $F^l$ .

We compared eigenvalues of the LPA system and of the full RDEs in the limit  $D_u \rightarrow 0$ ,  $D_v \rightarrow \infty$ . From Fig. 3(a) and (b), we see that LPA eigenvalues provide a reasonable asymptotic approximation of Turing eigenvalues. This confirms that Property 2 in Appendix A holds for this three component system. The significance of this result is that the full model exhibits responses that depend on spatial aspects of the system that are absent in homogeneous (well-mixed) variants of the model.

Further notice that between the branch points (BP) in Fig. 2 (b) and (c), the local eigenvalues are real and positive, indicating simple Turing instability. Between the Hopf and branch points, eigenvalues are complex conjugates with positive real part, corresponding to a traveling wave (oscillatory Turing) instability, as found in Yang et al. (2002) and Wang et al. (2007) for example. The LPA thus predicts four stability regimes. (a) Between  $k_0 = 0$  and the bifurcation labeled H, sufficiently large perturbations induce patterning (nonlinear instability). (b) In the range from H to BP, a wave instability is present. (c) Between the two BP bifurcations, a stationary Turing instability is present. (d) From H to  $k_0 = \infty$ , no patterning is possible.

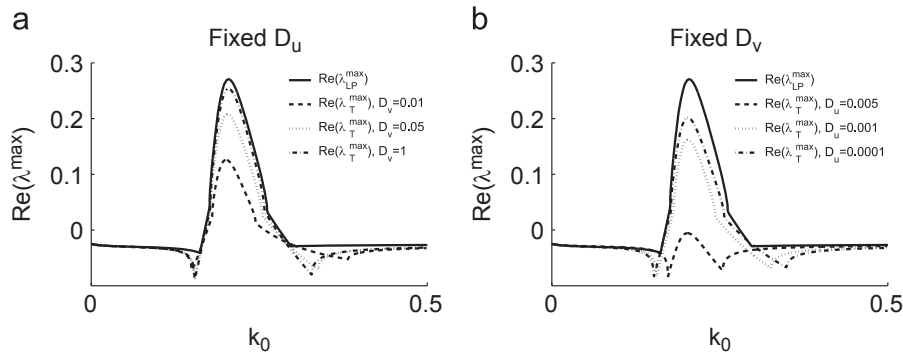


**Fig. 3.** In the limits (a)  $D_v$  (i.e.  $D_l$ )  $\rightarrow \infty$  and (b)  $D_u$  (i.e.  $D_A$ )  $\rightarrow 0$ , Turing maximal eigenvalues (dashed and dotted) approach LPA eigenvalues (solid). The real parts of  $\lambda^{\max}$  is plotted against  $k_0$ . In the given limits, the LPA and Turing eigenvalues agree well.

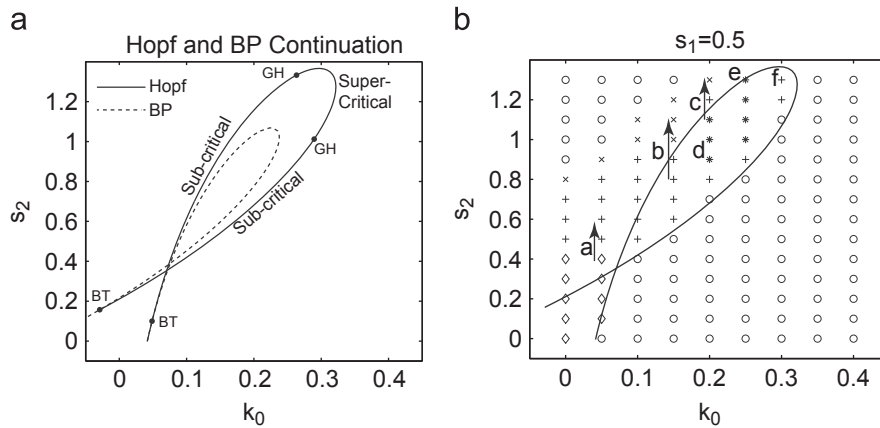


**Fig. 4.** Left: The  $s_2, k_0$  two-parameter continuation of the H and BP bifurcations seen in Fig. 2(c). GH and BT represent co-dimension 2 Generalized Hopf and Bogdanov–Takens bifurcations. At BT, the solid branch switches from being a neutral saddle to a Hopf bifurcation. At GH, the criticality of the Hopf curve changes.  $s_1=0.5$ ,  $\epsilon=0.1$  and all other parameters as in Table 1. Right: the same parameter plane showing classification of the resulting long-term dynamics into one of several patterns: no pattern (o), boundary localized ( $\diamond$ ), reflecting pulse (+), pulse trains (\*), and a single pulse ( $\times$ ). Arrows and letters indicate the parameter values corresponding to long term simulations in Fig. 5. The LPA  $s_2, k_0$  two-parameter continuation of the Hopf bifurcations (curves) is superimposed.

5.2.1. Role of conservation

Consider for the moment the actin-NPF model equation (2) with the quantity  $I$  fixed as a parameter. Then the remaining  $A, F$  system has an activator–inhibitor structure that can be shown to oscillate. This is the source of the Hopf bifurcation and corresponding oscillatory dynamics of the local variables  $A^l, F^l$ , for which  $I^g$  plays the role of a parameter (since  $I$  is fixed at its steady state value). The global variables  $A^g, I^g, F^g$ , on the other hand, satisfy the conservation law  $A^g + I^g = 1$  and evolve according to the kinetics of the well-mixed system, which exhibits a single stable steady state without oscillatory dynamics. We thus see that a minimum of two slow variables ( $A, F$ ) are required to produce the complex pair of local eigenvalues corresponding to oscillations on a local scale. The third fast variable ( $I$ ) is necessary to suppress these oscillations on the global scale and stabilize the well mixed system. In this way, the  $A, I, F$  model is a minimal system demonstrating the type of dynamics observed in our spatial model.

5.3. Two-parameter bifurcation analysis

In order to investigate the interplay between the activation parameter  $k_0$  and the F-actin negative feedback  $s_2$ , we next perform a two-parameter bifurcation analysis, tracking both the Hopf (H) and branch point (BP) bifurcations, Fig. 4. Interesting dynamics lie along a diagonal region in Fig. 4(a), where the activation and feedback are roughly balanced. While Fig. 2 (c) identifies both wave and Turing instabilities for  $s_2=0.7$ , there

is a region at higher  $s_2$  values where only wave instabilities occur. As  $s_2$  is increased further, the Turing region shrinks and terminates. This observation indicates that (a) stationary Turing instabilities are prominent at lower  $s_2$  values, (b) oscillatory wave instabilities take over at intermediate  $s_2$  values, and (c) yet higher  $s_2$  values stabilize the HSS.

For low values of  $s_2, k_0$ , in Fig. 4(a) the Hopf bifurcations are sub-critical and large amplitude oscillations result immediately upon crossing these bifurcation points. When  $s_2, k_0$  increase, the Hopf branch undergoes a Generalized Hopf bifurcation (GH), becoming super-critical. Bogdanov–Takens (BT) bifurcations represent the intersection of the Hopf and BP curves. For  $s_2$  below these bifurcation points, the H branch represents neutral saddles rather than an oscillatory bifurcation. As  $s_2$  is increased, the neutral saddles cross through the BP curve becoming true Hopf points.

5.4. Long term evolution of patterns

In order to gain insight about how predictions of LPA and standard stability analysis compare with actual long-term evolution of patterns, we carried out full numerical simulations of the model equations (2). We explored the simulated behavior (with default parameters as in Table 1), and compared the actual patterns observed to the regimes obtained in the LPA two-parameter continuation of Fig. 4(a). To do so, we used an automated classification algorithm (Holmes et al., 2012a) for broad pattern classification, as shown in Fig. 4(b).

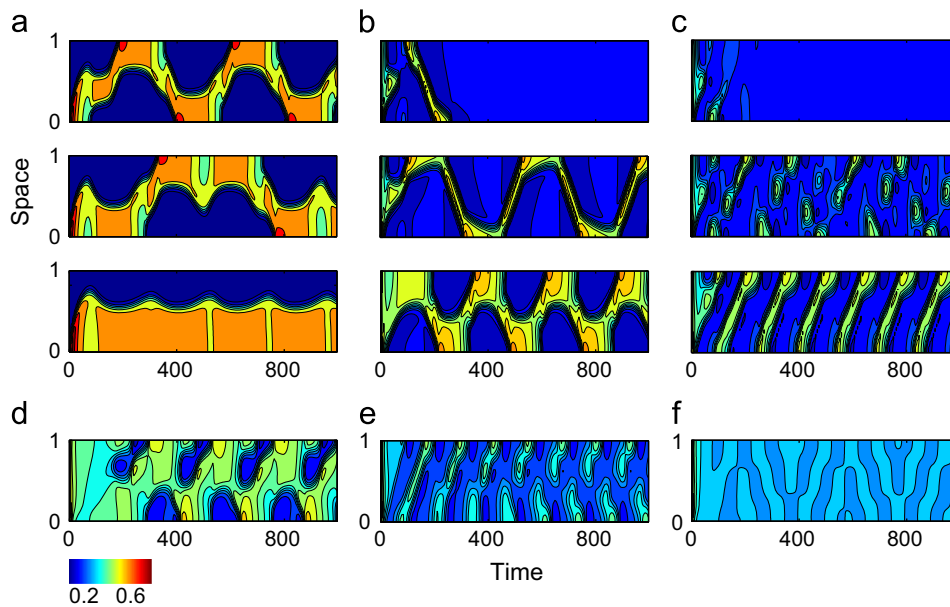


**Fig. 5.** Simulations of the full model, showing  $A(x, t)$  as intensity plots versus  $x$  (vertical) and  $t$  (horizontal) axes. (a–c): transitions represented by arrows (a–c) in Fig. 4b, ( $s_2$  increases from bottom to top in each column). (d–f) Exotic patterns at the borders of regimes, as in Fig. 4b. (a)  $k_0 = 0.05$ ,  $s_2 = 0.4, 0.56, 0.6$ , (b)  $k_0 = 0.15$ ,  $s_2 = 0.8, 1.02, 1.1$ , (c)  $k_0 = 0.2$ ,  $s_2 = 1.1, 1.24, 1.3$ , (d)  $k_0 = 0.2$ ,  $s_2 = 0.83$ , (e)  $k_0 = 0.25$ ,  $s_2 = 1.3$  (f)  $k_0 = 0.3$ ,  $s_2 = 1.36$  (see also Table 1).

For each  $s_2$ ,  $k_0$  grid point, a simulation is run and we indicate one of five basic behaviors: no pattern (o), boundary localized ( $\diamond$ ), reflecting pulse (+), pulse trains (\*), and a single pulse ( $\times$ ). As suggested by the LPA continuation curves, interesting dynamics occur along the diagonal in the  $s_2$ ,  $k_0$  plane, where activation ( $k_0$ ) and feedback mediated inactivation ( $s_2$ ) of the regulatory protein roughly balance. The labeled arrows in Fig. 4(b) correspond to simulations in Fig. 5.

We examined in greater detail some of the transitions between pattern types. Here we comment on several examples, indicated by the span and direction of arrows in Fig. 4(b). In each case, we explain how the pattern changes over a parameter sweep (base to tip of arrow). Then, we show these transitions (bottom to top) in correspondingly labeled panels in Fig. 5. The value  $s_2 = 0$  corresponds to pure wave-pinning and hence, to a polarized state. (a) For relatively low values of  $s_2$  and  $k_0$ , a transition from static to dynamic patterns is seen: As  $s_2$  increases, the polarized state first undergoes local oscillations at the boundary, and then transitions smoothly into a reflecting pulse solution. (b) At larger  $k_0$ ,  $s_2$  values, the width of the reflecting pulse decreases. Eventually, a single pulse traverses the domain once and terminates. (c) For larger  $s_2$ , an oscillating amplitude is superimposed on the traveling wave train. In both (b) and (c), the pulse is suppressed smoothly with increased  $s_2$ , eventually leading to transient dynamics. A few additional exotic patterns (d–f) are also shown in Fig. 5. We found that at higher values of  $s_2$  (not shown), there is complete suppression of dynamics.

Further comparing long-term behavior with the LPA bifurcation structure, we see that different wave regimes can be identified with distinct regimes depicted in the LPA. Wave trains are associated with a Turing bifurcation in which a pair of complex conjugate eigenvalues have a positive real part (“non-stationary Turing bifurcation”). The oscillatory nature of these waves arises as an instability of the HSS, and is predicted by linear stability analysis. In this sense, the wave trains occur “spontaneously” in response to small perturbations or noise. In contrast, reflecting waves occur either in (1) a stationary Turing regime (a single real positive eigenvalue) or (2) linearly stable regime with a threshold that can be breached by a sufficiently large perturbation. In the

stationary Turing regime, noise initiates patterning but without any propagation dynamics. Once this pattern grows, nonlinear effects become important and lead to propagation. Thus, reflecting waves are inherently a nonlinear phenomenon, and they can be either spontaneous or excitable. In both regimes (1) and (2), the dynamics of reflecting waves cannot be predicted based on linear stability analysis. We conclude that, while the LPA does not directly predict long-term patterns, it allows some inferences about how stability properties correlate with dynamics. In particular, LPA suggests that reflecting waves and wave trains are initiated in fundamentally distinct ways.

### 5.5. Pulse width/velocity

To further characterize how patterns change as the parameters of the model are varied, we investigated pulse width and velocity (for reflecting pulses and pulse trains). Results for  $k_0$  and  $s_2$  are shown in Fig. 6. Pulse width was computed at the half maximum and velocity was computed by tracking the location of the maximal value of  $A$  as a function of time and computing the slope of the resulting line. This width increases as the activation rate  $k_0$  increases (or as the negative feedback parameter  $s_2$  decreases), as expected. Wave speed decreases as  $k_0$  is increased (or as  $s_2$  is decreased) which is unusual, since wave velocities typically increase with activation rates. Both patterns, reflecting pulses and pulse trains, exhibit similar parameter dependence.

The dependencies of pulse velocity and width on parameters are particularly interesting as they depart from expectation. In classical wave propagation models such as FitzHugh Nagumo (compared to our model in Section 6), propagation velocity increases with an activation rate, in contrast to what we find here. We can explain this by noting that in our model, the rate of activation depends not only on the rate parameters  $k_0$ ,  $\gamma$ , but also on the available pool of inactive form  $I$ . As that pool is depleted, propagation velocity falls (Mori et al., 2008). Thus there is an inverse relationship between pulse width and velocity, larger pulses deplete the inactive pool further, slowing propagation. So paradoxically, increasing the rate of activation ( $k_0$ ) increases the depletion of this pool and slows propagation. Similarly, it is

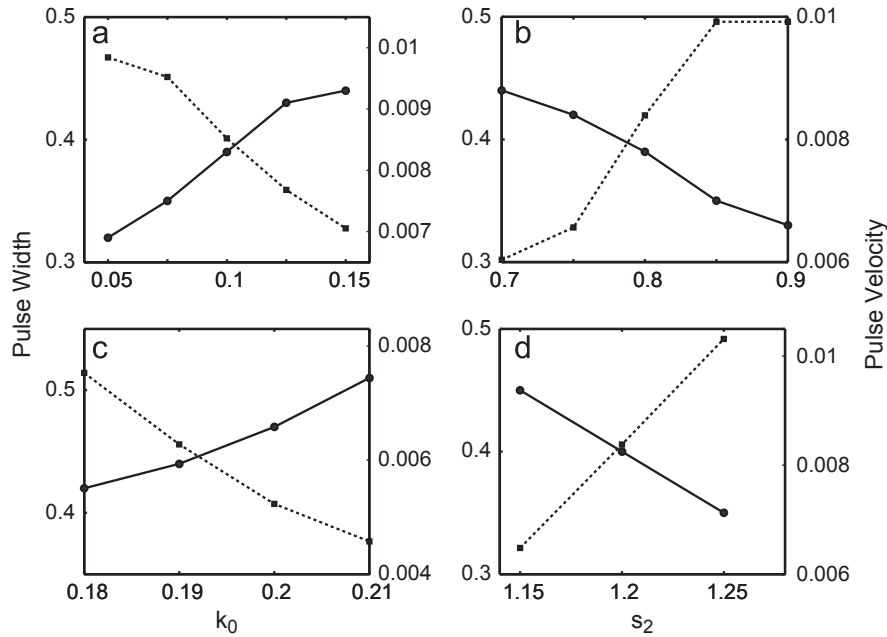


**Fig. 6.** Pulse width (solid) and velocity (dashed) versus  $k_0$  (left) and  $s_2$  (right) for reflecting pulses (top) and pulse trains (bottom). Width is measured at the pulse half maximum for A, and velocity is determined by plotting the position of the pulse maximum as a function of time and computing the slope. Parameters: (a)  $s_2 = 0.8$ , (b)  $k_0 = 0.1$ , (c)  $s_2 = 1.0$ , and (d)  $k_0 = 0.25$ . All other parameters are as in Table 1.

depletion of the inactive protein limits the width of the activated regions.

Fig. 7 supports this relationship. Fig. 7(a) shows that as the total pool of regulatory protein,  $T_{NPF}$ , is increased, the pulse width increases commensurately. This increase in pulse width depletes the pool of inactive NPF to roughly the same level at each value of  $T_{NPF}$  (data not shown). For this reason, while pulse velocity increases, it does so by a smaller fraction since the net activation rate remains roughly the same.

### 5.6. The F-actin (refractory) time scale, $\epsilon$

So far, we have explored the roles of activation rate and negative feedback parameters. Small values of  $\epsilon$  correspond to a slow F-actin response. Varying this parameter will increase or decrease the influence of the F-actin on its regulators, which corresponds to a change in the timescale for the slow (refractory) negative feedback. It is well known that the timescale of refractory negative feedback is an important determinant of oscillatory dynamics. Hence, we here explore the role of  $\epsilon$  and characterize the conditions required for these oscillatory bifurcations to occur.

In Appendices C.1 and C.2, we show that  $\epsilon$  does not affect the values of the steady state of the LPA-system  $q^* = (\bar{A}^g, \bar{I}^g, \bar{F}^g, \bar{A}^l, \bar{F}^l)$  but does affect stability. Briefly, the LPA Jacobian is in the form

$$J_{LP} = \begin{bmatrix} J_0 & 0 \\ J_{ext} & J_{loc} \end{bmatrix}, \quad \text{where } J_{loc} = \begin{bmatrix} H_1(A^l, F^l) & H_2(A^l, F^l) \\ \epsilon k_n & -\epsilon k_s \end{bmatrix} \quad (7)$$

$J_0$  is the well mixed Jacobian (A.1), and  $J_{loc}$  is the Jacobian of the equations involving the local variables. Both  $H_i$  (Eq. (C.7)) are independent of  $\epsilon$ .  $J_{ext}$  does not affect eigenvalues due to the block lower triangular structure. Since eigenvalues of  $J_0$  are negative,  $J_{loc}$  alone governs the appearance of Hopf bifurcations and oscillations, and its eigenvalues are

$$\lambda_{\pm} = \frac{1}{2} (H_1 - \epsilon k_s) \pm \frac{1}{2} \sqrt{(H_1 + \epsilon k_s)^2 - 4\epsilon k_n H_2}. \quad (8)$$

(These explicitly depend on  $\epsilon$ .) The conditions for a Hopf bifurcation are now

$$\mathcal{I}(\lambda) = (H_1 + \epsilon k_s)^2 - 4\epsilon k_n H_2 < 0, \quad \mathcal{R}(\lambda) = H_1 - \epsilon k_s = 0 \quad (9)$$

which can be reformulated as

$$\epsilon = H_1/k_s =: B_1, \quad \epsilon < \frac{k_n}{k_s^2} H_2 =: B_2. \quad (10)$$

For a fixed set of parameters excluding  $\epsilon$ , the above implies that there is a maximum value  $\epsilon^*$  where  $B_1 \leq B_2$ , for which a Hopf bifurcation exists. As an illustration, we plot  $\epsilon = B_{1,2}(k_0)$  for two parameter sets in Fig. 8 (a) and (c) and LPA diagrams for  $\epsilon = 0.3$  in Fig. 8 (b) and (d). A Hopf bifurcation exists wherever the curve  $\epsilon = B_1$  lies below the curve  $\epsilon = B_2$ . Where  $B_1 > B_2$ , the  $B_1$  curve represents saddle points without oscillatory instabilities. The associated LPA diagrams in panels (b) and (d) showing the presence (or absence) of Hopf bifurcations are consistent with the results of this eigenvalue analysis.

Thus, as the relative timescale of the refractory negative feedback  $\tau = 1/\epsilon$  decreases, oscillatory dynamics are suppressed. Intuitively, the refractory timescale should be long enough that large deviations of  $A^l$  driven by activation are achieved before suppression by feedback. This timescale dependence often occurs in single refractory feedback systems, such as the FitzHugh Nagumo (FHN) model. While these conclusions are based on LPA, the fact that local eigenvalues approximate eigenvalues of the linearized RDEs, means that oscillatory linear instabilities would be seen in the original RDE system.

This refractory timescale does not affect the branch point (BP) bifurcations since those result purely from the presence of local branches representing  $\epsilon$  independent steady states.

We explored the effect of  $\epsilon$  on long term behavior. Keeping other parameters at their default values (Table 1), we varied  $\epsilon$  from 0.001 to 0.5 in Fig. 9(a). When  $\epsilon$  is small, F-actin responds slowly, somewhat decoupling the regulatory protein equations. Consequently, that system exhibits wave pinning dynamics, and static

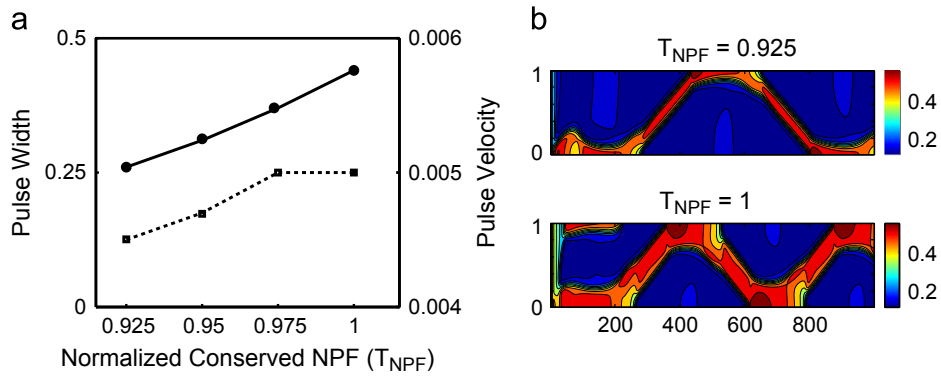


**Fig. 7.** The effects of the total amount of regulatory protein  $T_{NPF}$  on pulse propagation. (a) Pulse width (solid) and velocity (dashed) as a function of  $T_{NPF}$ . (b) Intensity plot of  $A$  at the two endpoints  $T_{NPF} = 0.925, 1$  respectively. Parameters are  $k_0 = 0.15$ ,  $s_1 = 0.7$ ,  $s_2 = 0.6$  with all others as in Table 1.

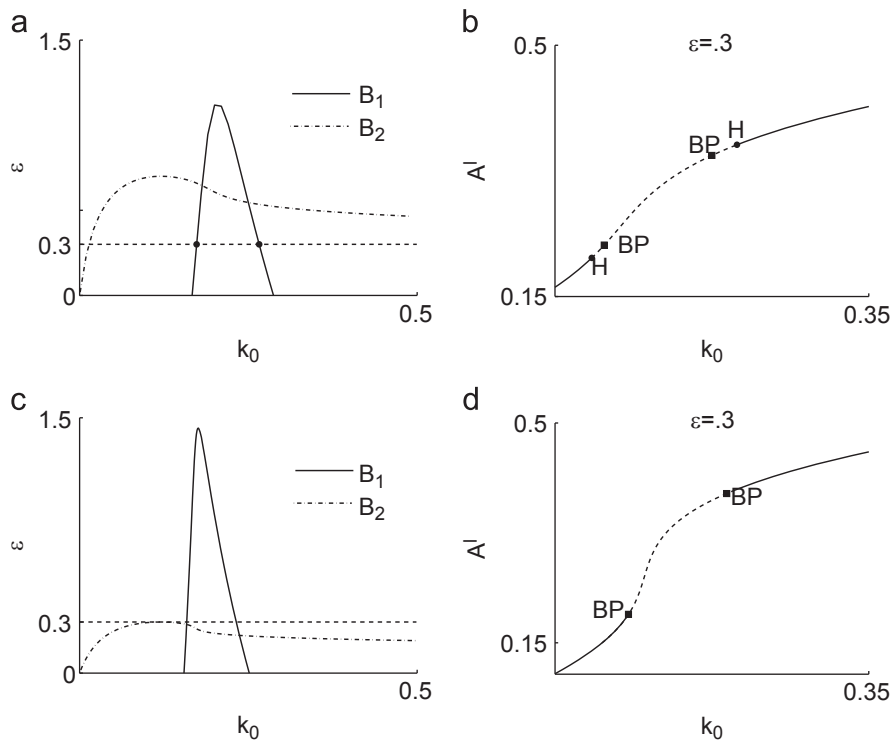


**Fig. 8.** The timescale of F-actin dynamics affects the presence and locations of Hopf bifurcations in the LPA system and oscillatory dynamics in the original RDEs. *Left:* plot of  $B_1(k_0)$  and  $B_2(k_0)$  of (10) for (a)  $s_1 = s_2 = 0.7$ , (c)  $s_1 = 0.9$  and  $s_2 = 0.3$  (Other parameters as in Table 1). Horizontal dashed lines are values of  $\epsilon$  corresponding to LPA diagram (b) and (d). Hopf bifurcations correspond to  $(k_0, \epsilon)$  values on the  $B_1$  curve below  $B_2$ . Points on the  $B_1$  curve above  $B_2$  represent saddles. Heavy dots on the  $B_1$  curve in (a) correspond to Hopf points in (b). In (b) and (d), we show LPA bifurcation plots for the parameter sets corresponding to (a) and (c) respectively with  $\epsilon = 0.3$ .

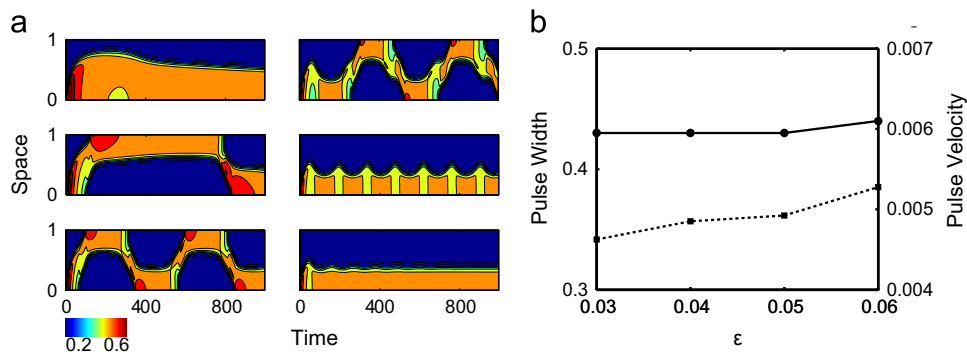


**Fig. 9.** The effect of the refractory feedback rate  $\epsilon$ . (a) Intensity plots of  $A$ . The  $\epsilon$  values from top to bottom, left to right are 0.001, 0.01, 0.05, 0.11, 0.19, 0.29. Other parameters as for reflecting pulses in Table 1. (b) Pulse width (solid) and velocity (dashed) as a function of  $\epsilon$  for reflecting waves.

patterns result (panel a, top left). For large values of  $\epsilon$ , actin polymerization and regulatory protein dynamics occur on the same timescale, also resulting in static patterns (panel a, bottom right). Patterning is most dynamic between these extremes.

Finally, we asked how  $\epsilon$  affects pulse width and velocity. Results for reflecting pulses are shown in Fig. 9b. Similar results were found for pulse trains (not shown). Increasing  $\epsilon$  by a factor of 2 results in a 20% increase in the velocity, as expected, but hardly affects the width of the pulse (a mere 2% change). The latter result is counterintuitive, since a larger feedback rate  $\epsilon$  should suppress the trailing edge faster, leading to smaller activated regions.

## 6. Comparison to FitzHugh Nagumo model

It is illuminating to compare our F-actin regulation model with the FitzHugh Nagumo (1969) model, a well-known elementary model for excitation waves. Both models have a nonlinear wave generator, and a refractory negative feedback.

In the FHN system, one equation consist of nonlinear (“cubic”) kinetics that engenders bistability and hysteresis. A second linear equation describes the evolution of a “recovery” (or refractory) variable whose feedback leads to cycling around the hysteretic loop. The system has limit cycle oscillations even in the space-independent case. Diffusion spreads the excitation in space, spawning a traveling wave-front separating regions of low and high activity that sweeps entirely through the domain. Refractory negative feedback suppresses the trailing edge of that wave, producing a traveling pulse with a spatially localized high state separating low states on either side. For this model, pulse velocity increases with respect to an activation rate that resembles the activation parameter  $k_0$ , and pulse width decreases as an  $\epsilon$  like refractory rate parameter increases.

In the F-actin regulation model, our results indicate that stability properties and long term dynamics of (2) are not merely inherited from the behavior of the space-free system. In the parameter range of interest, and in absence of feedback ( $s_2 = 0$ ), that underlying system has a single steady state. Turning on the refractory feedback ( $s_2 > 0$ ) does not induce limit cycle oscillations. Rather, diffusion plays a vital role in determining the wave and pulse behavior. So, in contrast to the standard FHN system, the reaction kinetics alone do not sustain oscillatory dynamics; in fact, diffusion is required for wave formation. The reason for this is that in contrast to the FHN system, instead of traditional bistability associated waves, the wave generating  $A, I$  system of proteins sustain a “wave pinning” behavior, for which diffusion is a key ingredient. Refractory feedback interacts with this form of wave generation to produce traveling wave and Turing bifurcations of the full RDEs. Conservation of  $A+I$  is a key feature that gives rise to these interesting stability properties. With  $I$  held fixed,  $A$  and  $F$  exhibit typical activator/inhibitor oscillations on a local spatial scale (as demonstrated by the local variables). The conservative dynamics of  $I$  on the other hand stabilize the spatially homogeneous system.

Furthermore, as shown above, the long-term dynamics of the F-actin regulation model and those of FHN differ significantly. In our model, we find both persistent and transient dynamics in linearly stable parameter regimes, whereas FHN shows only transient single pulse dynamics. Second, polarized patterns, boundary oscillations, and reflecting wave dynamics are not exhibited by the FHN system. Third, pulse velocities depend inversely on the regulatory protein activation parameter  $k_0$  rather than directly. Fourth, the size of an activated region is insensitive to the refractory timescale  $\epsilon$ . Finally, our results on the relationship between the total pool of regulatory protein,  $T_{NPF}$ , and pulse width and velocity (Fig. 7) also demonstrate the importance of

conservation of the total amount of regulating protein ( $T_{NPF}$ ). This is the key structural property differentiating our model from FHN.

## 7. Discussion

At present, it is not certain whether actin waves are secondary phenomena, or whether they have functional significance to cell behavior. It has been speculated that the waves of F-actin aid cells to explore their environment (Weiner et al., 2007; Schroth-Diez et al., 2009), engulf particles (Gerisch, 2010), and/or organize cell edge protrusion (Driscoll et al., 2012). Whether or not such waves have functional significance, their existence informs models for F-actin and its regulators. Here we have shown that a minimal model, combining a caricature of small GTPases (the “wave pinning”  $A, I$  system) with feedback to/from F-actin is capable of producing a rich diversity of patterns: static polarization, reflecting waves, wave trains, transient pulses, and persistent boundary oscillations, with a variety of smooth transitions between them. Further, it is one of the simplest models exhibiting such behavior.

In analyzing regimes of behavior of the model, we introduced and applied the local perturbation analysis (LPA), a method for determining nonlinear stability properties. This method rests on the observation that for systems with a large diffusion disparity, the response to an arbitrarily tall but spatially localized perturbation can be approximated by a set of ODEs for global (fast) and local (slow) variables. LPA bifurcation plots (Figs. 2 and 4a) then provide useful information about growth or decay of that perturbation. While the predictions are (like all stability analyses) short-term, they help to highlight how patterning is initiated: whether through arbitrarily small amplitude stimuli, or as threshold responses to perturbations of some finite size. In this sense, LPA provides a combination of linear and nonlinear stability information.

It is worth mentioning that LPA is uniquely suited to analyze biologically motivated systems. For one thing, it is capable of detecting both linear and nonlinear patterning phenomena. Linear and nonlinear methods can in some cases be combined to provide similar or even more complete information. However this is usually possible only in specific situations where functional forms are amenable to analysis. Furthermore, such methods are usually only applicable in systems involving a small number of variables. We have applied LPA to substantially larger and more complex systems without particular difficulty. Examples can be found in Holmes et al. (2012b), Marée et al. (2006, 2012). Since LPA takes advantage of existing bifurcation software, the technical/computational “cost” of its implementation is low compared to other methods.

Applied to the actin-waves model, LPA reveals two distinct linearly unstable regimes (both stationary Turing and oscillatory wave instabilities, in agreement with classical linear analysis), and a third regime whose homogeneous steady state is unstable to a sufficiently large perturbation (not detected by linear methods). Simulations of the full model confirmed those LPA predictions. For example, the two-parameter LPA bifurcation diagram (Fig. 4) predicts that interesting dynamics occur when there is a rough balance between activation ( $k_0$ ) and inactivation ( $s_2$ ) parameters, in agreement with simulations. Wave trains were found to correlate with the wave instability detected by the LPA, and reflecting waves with the stationary Turing instability and threshold patterning regimes. Further analysis showed oscillatory instabilities require the actin feedback rate ( $\epsilon$ ) to be smaller than the protein activation rate.

While aspects of the model were motivated by the refractory and bistable components of the FitzHugh Nagumo model, we showed that its behavior contrasts in important ways. For one

thing, our model has no inherent oscillatory features when the system is well-mixed and the spatial distribution is essential. Second, pattern regimes are significantly more diverse than those found in the FHN model. Third, pulse width and velocities depend in counterintuitive ways on parameters. Finally, the conservation of  $A+I$  in our model appears to be a distinguishing feature that is vitally important in determining these dynamics.

We can use several features of the model to suggest experimental tests. Among these are the role of conservation of the regulatory proteins and the predicted inverse relationship between pulse width and velocity. First, we predict that any perturbation that increases NPF activation would lead to wider, slower waves. Consequently, increasing GEF activation or overexpressing a GEF (which corresponds to increasing the basal activity  $k_0$ , of NPFs such as Cdc42 or Rac) should produce this effect. Conversely, overexpressing or increasing GAP activity (identified with increasing the rate of inactivation of GTPases,  $s_1$ ) should have the opposite effect, producing thinner, faster waves. Perturbations that magnify F-actin mediated feedback, indicative of an increase in  $s_2$  should produce this result. Overexpression of Arp2/3, WASP, or the Wave complex (identified with an increase in  $k_n$ ) would, by enhancing F-actin production, also lead to thinner, faster waves. Finally, overexpressing GTPases such as Cdc42 or Rac, which is equivalent to increasing  $T_{NPF}$  should lead to wider waves while having a modest effect on propagation velocity.

**Acknowledgments**

The authors acknowledge the support from NSERC postgraduate fellowship to MD. WRH has been partially supported by NIH grant P50GM76516.

**Appendix A. Comparison of local perturbation analysis (LPA) and linear stability (Turing) analysis**

Here we provide details for the comparison of the nonlinear LPA stability analysis method to the linear Turing stability analysis. Consider the homogeneous steady state,  $(u^s, v^s)$  of (3). Linear stability to spatially nonuniform perturbations is determined by eigenvalues of

$$J_k = \begin{bmatrix} f_u & f_v \\ g_u & g_v \end{bmatrix}_{(u^s, v^s)} - (k\pi)^2 \begin{bmatrix} D_u & 0 \\ 0 & D_v \end{bmatrix}. \tag{A.1}$$

These eigenvalues are growth rates of a small periodic perturbation of the form  $\cos(k\pi x)$ . Define  $\{\lambda_i^k\}_i$  to be those eigenvalues.

Note that  $(u^s, v^s, u^l) = (u^s, v^s, u^s)$  is a fixed point of the LPA-ODE's (5). Thus stability of the HSS to a localized perturbation (LPA stability) is determined by eigenvalues of (6), reproduced below

$$J_{LP} = \begin{bmatrix} f_u(u^s, v^s; p) & f_v(u^s, v^s; p) & 0 \\ g_u(u^s, v^s; p) & g_v(u^s, v^s; p) & 0 \\ 0 & f_v(u^s, v^s; p) & f_u(u^s, v^s; p) \end{bmatrix}. \tag{A.2}$$

*Property 1:* LPA recapitulates linear stability results for the well-mixed system (4).

*Verification:* notice that (5a) and (5b) decouple and represent the well-mixed system (4). As a result, (A.2) is block lower triangular with the top left block representing  $J_0$  (A.1). So  $\{\lambda_i^0\}_i$  are eigenvalues of (A.2) Nicholson (1995) and any instabilities associated with the  $k=0$  mode (well-mixed instabilities) are found by LPA. From here on, we refer to  $\{\lambda_i^0\}_i$  as well-mixed eigenvalues.

*Property 2:* LPA recapitulates linear stability results for the full reaction-diffusion system (Turing stability analysis).

*Verification for two variable systems:* note that the remaining eigenvalues of  $J_{LP}$  are determined precisely by the eigenvalues of

$f_u(u^s, v^s; p)$ . Define these to be  $\{\lambda_j^{LP}\}_j$ . We compare the Turing eigenvalues  $\{\lambda_i^k\}$  with the remaining LPA eigenvalues  $\{\lambda_j^{LP}\}_j$  in the extreme diffusion regime where the LPA is valid. A simplified setting with one fast and one slow diffusing variable is considered. In this setting, the eigenvalues  $\lambda_1^k, \lambda_2^k$  are roots of the characteristic polynomial

$$(f_u - \pi^2 k^2 D_u - \lambda)(g_v - \pi^2 k^2 D_v - \lambda) - f_v g_u = 0. \tag{A.3}$$

In the LPA regime,  $D_u < 1 < D_v$ , these roots satisfy

$$\lambda_1^k = O(1), \quad \lambda_2^k = -\pi^2 k^2 D_v + O(1). \tag{A.4}$$

Then clearly  $\lambda_2^k$  has negative real part independent of the system parameters and does not contribute to stability properties. Consider instead the  $O(1)$  eigenvalue. Substituting into (A.3)

$$(f_u - \pi^2 k^2 D_u - \lambda_1^k) \cdot O(D_v) - f_v g_u = 0. \tag{A.5}$$

Thus,  $\lambda_1^k = f_u(u^s, v^s; p) - \pi^2 k^2 D_u + O(D_v^{-1}) \approx f_u(u^s, v^s; p) = \lambda_1^{LP}$  in the relevant limit. This Turing eigenvalue contributes to stability and as we have shown here, is approximated by an LPA eigenvalue. We will refer to  $\{\lambda_j^{LP}\}_j$  as “local” eigenvalues. For the  $3 \times 3$  (A, I, F) system, where this verification does not apply, we show numerically that Result 2 still holds.

**Appendix B. Nondimensionalizing the model**

The equations of the full actin waves model are

$$\frac{\partial A}{\partial t} = f(A, I, F) + \tilde{D}_A \Delta A, \tag{B.1a}$$

$$\frac{\partial I}{\partial t} = -f(A, I, F) + \tilde{D}_I \Delta I, \tag{B.1b}$$

$$\frac{\partial F}{\partial t} = h(A, F), \tag{B.1c}$$

with

$$f(A, I, F) = \tilde{\delta} \left[ \left( k_0 + \gamma \frac{A^3}{\tilde{A}_0^3 + A^3} \right) I - \left( s_1 + s_2 \frac{F}{\tilde{F}_0 + F} \right) A \right], \tag{B.1d}$$

$$h(A, F) = \tilde{\epsilon} (\tilde{k}_n A - k_s F). \tag{B.1e}$$

Equations for A, I imply that

$$\int_0^L (A(x, t) + I(x, t)) dx = \tilde{T}_{NPF} \tag{B.2}$$

is constant.

We translate the model into dimensionless form by rescaling the variables as follows:

$$\bar{A} = \frac{A}{\tilde{T}_{NPF}}, \quad \bar{I} = \frac{I}{\tilde{T}_{NPF}}, \quad \bar{F} = \frac{F}{\tilde{F}_0}, \quad \bar{t} = \tilde{\delta} t, \quad \bar{x} = \frac{x}{L}. \tag{B.3}$$

After making these substitutions and dropping the bars, the resulting nondimensional equations become (2) with

$$A_0 = \frac{\tilde{A}_0}{\tilde{T}_{NPF}}, \quad D_A = \frac{\tilde{D}_A}{\tilde{\delta} L^2}, \quad D_I = \frac{\tilde{D}_I}{\tilde{\delta} L^2}, \quad \epsilon = \frac{\tilde{\epsilon}}{\tilde{\delta}}, \quad k_n = \frac{\tilde{k}_n \tilde{T}_{NPF}}{\tilde{F}_0} \tag{B.4}$$

and

$$\int_0^1 (A(x, t) + I(x, t)) dx = T_{NPF} = 1. \tag{B.5}$$

Note that while total protein amounts have been normalized to one, we will allow  $T_{NPF}$  to vary in order to investigate the effects of protein amounts on dynamics. In this way,  $T_{NPF}$  parameterizes total protein levels relative to a typical amount  $\tilde{T}_{NPF}$ . Further note that several rate parameters from the original model ( $k_0, \gamma, s_1, s_2, k_n, k_s$ ) were

already dimensionless as a result of aggregating the timescale information into  $\tilde{\delta}, \tilde{\epsilon}$ .

### Appendix C. LPA equations for the model

The LPA equations for the model are

$$\frac{dA^g}{dt} = f(A^g, I^g, F^g), \quad \frac{dA^l}{dt} = f(A^l, I^g, F^l), \quad (C.1a)$$

$$\frac{dF^g}{dt} = \epsilon h(A^g, F^g), \quad \frac{dF^l}{dt} = \epsilon h(A^l, F^l), \quad (C.1b)$$

$$\frac{dI^g}{dt} = -f(A^g, I^g, F^g) \quad (C.1c)$$

with kinetics as defined previously in (2).

#### C.1. LPA system steady states

The steady state of the LPA-system  $q^* = (\bar{A}^g, \bar{I}^g, \bar{F}^g, \bar{A}^l, \bar{F}^l)$  is independent of  $\epsilon$ . It satisfies

$$A^g|_{q^*} = 0 \text{ or } I^g|_{q^*} = 0 \Rightarrow \left( k_0 + \gamma \frac{(\bar{A}^g)^3}{A_0^3 + (\bar{A}^g)^3} \right) \bar{I}^g = \left( s_1 + s_2 \frac{\bar{F}^g}{1 + \bar{F}^g} \right) \bar{A}^g, \quad (C.2)$$

$$A^l|_{q^*} = 0 \Rightarrow \left( k_0 + \gamma \frac{(\bar{A}^l)^3}{A_0^3 + (\bar{A}^l)^3} \right) \bar{I}^g = \left( s_1 + s_2 \frac{\bar{F}^l}{1 + \bar{F}^l} \right) \bar{A}^l, \quad (C.3)$$

$$F^g|_{q^*} = 0 \Rightarrow \bar{F}^g = \frac{k_n}{k_s} \bar{A}^g, \quad F^l|_{q^*} = 0 \Rightarrow \bar{F}^l = \frac{k_n}{k_s} \bar{A}^l. \quad (C.4)$$

Further, using conservation ( $I^g + A^g = T_{NPF}$ ), we can eliminate  $I_g$ . Then, after some algebra, the steady states satisfy

$$\begin{aligned} \bar{A}^g \left( s_1 + s_2 \frac{k_n \bar{A}^g}{k_s + k_n \bar{A}^g} \right) \left( k_0 + \gamma \frac{(\bar{A}^g)^3}{A_0^3 + (\bar{A}^g)^3} \right)^{-1} \\ = \bar{A}^l \left( s_1 + s_2 \frac{k_n \bar{A}^l}{k_s + k_n \bar{A}^l} \right) \left( k_0 + \gamma \frac{(\bar{A}^l)^3}{A_0^3 + (\bar{A}^l)^3} \right)^{-1}. \end{aligned} \quad (C.5)$$

Clearly one solution satisfies  $\bar{A}^l = \bar{A}^g, \bar{F}^l = \bar{F}^g$  as expected, corresponding to the HSS.

#### C.2. LPA system stability

We compute the Jacobian of the LPA system equation (C.1) and find

$$J_{LP} = \begin{bmatrix} J_0 & 0 \\ J_{ext} & J_{loc} \end{bmatrix}, \quad \text{where } J_{loc} = \begin{bmatrix} H_1(A^l, F^l) & H_2(A^l, F^l) \\ \epsilon k_n & -\epsilon k_s \end{bmatrix}, \quad (C.6)$$

$J_0$  is the well mixed Jacobian (A.1),  $J_{ext}$  is extraneous and does not affect eigenvalues, and

$$H_1(A^l, F^l) = \frac{3\gamma A_0^3 (A^l)^2}{(A_0^3 + (A^l)^3)^2} (T_{NPF} - A^g) - \left( s_1 + s_2 \frac{F^l}{1 + F^l} \right) = \frac{\partial f}{\partial A^l}, \quad (C.7)$$

$$H_2(A^l, F^l) = -\frac{s_2 A^l}{(1 + F^l)^2} = \frac{\partial f}{\partial F^l}. \quad (C.8)$$

### Appendix D. Numerical implementation

To explore stability regimes and compare predictions of the analytic methods, we carried out a bifurcation analysis of the ODEs corresponding to the LPA and the well-mixed system. This

computation is carried out using the bifurcation package Matcont (Dhooge et al., 2003) of Matlab (MathWorks Inc.). Computation of Turing eigenvalues, LPA eigenvalues, and quantities associated with the refractory timescale  $\epsilon$  were performed using Mathematica (Wolfram Research). To track the long-term evolution of these patterns we carried out numerical simulations of the full RDEs, (2) in 1D using a Crank–Nicholson discretization scheme in Matlab.

### References

- Abram, C., Lowell, C., 2009. The ins and outs of leukocyte integrin signaling. *Annu. Rev. Immunol.* 27, 339.
- Bretschneider, T., Diez, S., Anderson, K., Heuser, J., Clarke, M., Mueller-Taubenberger, A., Koehler, J., Gerisch, G., 2004. Dynamic actin patterns and Arp2/3 assembly at the substrate-attached surface of motile cells. *Curr. Biol.* 14, 1–10.
- Bretschneider, T., Anderson, K., Ecke, M., Müller-Taubenberger, A., Schroth-Diez, B., Ishikawa-Ankerhold, H., Gerisch, G., 2009. The three-dimensional dynamics of actin waves, a model of cytoskeletal self-organization. *Biophys. J.* 96, 2888–2900.
- Calderwood, D., Shattil, S., Ginsberg, M., 2000. Integrins and actin filaments: reciprocal regulation of cell adhesion and signaling. *J. Biol. Chem.* 275, 22607–22610.
- Cantrell, R., Cosner, C., 2004. *Spatial Ecology via Reaction-Diffusion Equations*. Wiley.
- Carlsson, A., 2010a. Dendritic actin filament nucleation causes traveling waves and patches. *Phys. Rev. Lett.* 104, 228102.
- Carlsson, A., 2010b. Actin dynamics: from nanoscale to microscale. *Annu. Rev. Biophys.* 39, 91–110.
- Cross, M., Hohenberg, P., 1993. Pattern formation outside of equilibrium. *Rev. Mod. Phys.* 65, 851–1112.
- Dawes, A., Edelstein-Keshet, L., 2007. Phosphoinositides and rho proteins spatially regulate actin polymerization to initiate and maintain directed movement in a one-dimensional model of a motile cell. *Biophys. J.* 92, 744–768.
- Dhooge, A., Govaerts, W., Kuznetsov, Y., 2003. Matcont: a Matlab package for numerical bifurcation analysis of ODEs. *ACM TOMS* 29, 141–164.
- Dobrovinski, K., Kruse, K., 2008. Cytoskeletal waves in the absence of molecular motors. *Europhys. Lett.* 83, pp. 18003p1–6.
- Dobrovinski, K., Kruse, K., 2011. Cell motility resulting from spontaneous polymerization waves. *Phys. Rev. Lett.* 107, 258103.
- Driscoll, M.K., McCann, C., Kopace, R., Homan, T., Fourkas, J.T., Parent, C., Losert, W., 2012. Cell shape dynamics: from waves to migration. *PLoS Comput. Biol.* 8, e1002392.
- FitzHugh, R., 1969. *Mathematical Models of Excitation and Propagation in Nerve*, vol. 1. McGraw-Hill, New York, pp. 1–85.
- Gerisch, G., 2010. Self-organizing waves that simulate phagocytic cup structures. *BMC Biophys.* 3 (7).
- Gerisch, G., Bretschneider, T., Müller-Taubenberger, A., Simmeth, E., Ecke, M., Diez, S., Anderson, K., 2004. Mobile actin clusters and traveling waves in cells recovering from actin depolymerization. *Biophys. J.* 87, 3493–3503.
- Gollub, J., Langer, J., 1999. Pattern formation in nonequilibrium physics. *Rev. Mod. Phys.* 71, 396–403.
- Grieneisen, V., 2009. *Dynamics of Auxin Patterning in Plant Morphogenesis*. Ph.D. Thesis, University of Utrecht.
- Hall, A., 1998. Rho GTPases and the actin cytoskeleton. *Science* 279, 509–514.
- Holmes, W., Carlsson, A., Edelstein-Keshet, L., 2012a. Regimes of wave type patterning driven by refractory actin feedback: transition from static polarization to dynamic wave behaviour. *Phys. Biol.* 9, 046005.
- Holmes, W., Lin, B., Levchenko, A., Edelstein-Keshet, L., 2012b. Modelling cell polarization driven by synthetic spatially graded Rac activation. *PLoS Comput. Biol.* 8, e1002366.
- Iglesias, P., Devreotes, P., 2012. Biased excitable networks: how cells direct motion in response to gradients. *Curr. Opin. Cell Biol.* 24, 245–253.
- Iron, D., Ward, M., 2000. A metastable spike solution for a nonlocal reaction diffusion model. *SIAM J. Appl. Math.* 60, 778–802.
- Jilkine, A., Marée, A.F., Edelstein-Keshet, L., 2007. Mathematical model for spatial segregation of the Rho-Family GTPases based on inhibitory crosstalk. *Bull. Math. Biol.* 69, 1943–1978.
- Machacek, M., Hodgson, L., Welch, C., Elliott, H., Pertz, O., Nalbant, P., Abell, A., Johnson, G.L., Hahn, K.M., Danuser, G., 2009. Coordination of Rho GTPase activities during cell protrusion. *Nature* 461, 99–103.
- Mackay, D., Hall, A., 1998. Rho GTPases. *J. Biol. Chem.* 273, 20685–20688.
- Maini, P., Painter, K., Chau, H., 1997. Spatial pattern formation in chemical and biological systems. *J. Chem. Soc. Faraday Trans.* 93, 3601–3610.
- Marée, A., Jilkine, A., Dawes, A., Grieneisen, V., Edelstein-Keshet, L., 2006. Polarization and movement of keratocytes: a multiscale modelling approach. *Bull. Math. Biol.* 68, 1169–1211.
- Marée, A., Grieneisen, V., Edelstein-Keshet, L., 2012. How cells integrate complex stimuli: The effect of feedback from phosphoinositides and cell shape on cell polarization and motility. *PLoS Comput. Biol.* 8.

- Millius, A., Dandekar, S., Houk, A., Weiner, O., 2009. Neutrophils establish rapid and robust wave complex polarity in an actin-dependent fashion. *Curr. Biol.* 19, 253–259.
- Mori, Y., Jilkine, A., Edelstein-Keshet, L., 2008. Wave-pinning and cell polarity from a bistable reaction-diffusion system. *Biophys. J.* 94, 3684–3697.
- Mori, Y., Jilkine, A., Edelstein-Keshet, L., 2011. Asymptotic and bifurcation analysis of wave-pinning in a reaction-diffusion model for cell polarization. *SIAM J. Appl. Math.* 71, 1401–1427.
- Murray, J., 1981. A pre-pattern formation mechanism for animal coat markings. *J. Theor. Biol.* 88, 161–199.
- Nicholson, W., 1995. *Linear Algebra with Applications*, vol. 275. PWS Publishing Company.
- Nishiura, Y., 1982. Global structure of bifurcating solutions of some reaction-diffusion systems. *SIAM J. Appl. Math.* 13, 555–593.
- Okubo, A., Levin, S., 2002. *Diffusion and Ecological Problems*. Springer.
- Ridley, A., 2006. Rho GTPases and actin dynamics in membrane protrusions and vesicle trafficking. *Trends Cell Biol.* 16, 522–529.
- Rubinstein, B., Slaughter, B., Li, R., 2012. Weakly nonlinear analysis of symmetry breaking in cell polarity models. *Phys. Biol.* 9, 045006.
- Sasaki, A., Chun, C., Takeda, K., Firtel, R., 2004. Localized Ras signaling at the leading edge regulates PI3K, cell polarity, and directional cell movement. *J. Cell Biol.* 167, 505–518.
- Sasaki, A., Janetopoulos, C., Lee, S., Charest, P., Takeda, K., Sundheimer, L., Meili, R., Devreotes, P., Firtel, R., 2007. G protein-independent Ras/PI3K/F-actin circuit regulates basic cell motility. *J. Cell Biol.* 178, 185–191.
- Schroth-Diez, B., Gerwig, S., Ecke, M., Hegerl, R., Diez, S., Gerisch, G., 2009. Propagating waves separate two states of actin organization in living cells. *HFSP J.* 3, 412–427.
- Segel, L., Jackson, J., 1972. Dissipative structure: an explanation and an ecological example. *J. Theor. Biol.* 37, 545–559.
- Sit, S., Manser, E., 2011. Rho GTPases and their role in organizing the actin cytoskeleton. *J. Cell Sci.* 124, 679–683.
- Turing, A., 1952. The chemical theory of morphogenesis. *Philos. Trans. R. Soc.* 237, 37–72.
- Vicker, M., 2002a. F-actin assembly in dictyostelium cell locomotion and shape oscillations propagates as a self-organized reaction-diffusion wave. *FEBS Lett.* 510, 5–9.
- Vicker, M., 2002b. Eukaryotic cell locomotion depends on the propagation of self-organized reaction-diffusion waves and oscillations of actin filament assembly. *J. Exp. Cell Res.* 275, 54–66.
- Walther, G.R., Marée, A.F., Edelstein-Keshet, L., Grieneisen, V.A., 2012. Deterministic versus stochastic cell polarisation through wave-pinning. *Bull. Math. Biol.* 74, 2570–2599.
- Wang, W., Liu, Q., Jin, Z., 2007. Spatiotemporal complexity of a ratio-dependent predator-prey system. *Phys. Rev. E* 75, 051913.
- Weiner, O., Marganski, W., Wu, L., Altschuler, S., Kirschner, M., 2007. An actin-based wave generator organizes cell motility. *PLoS Biol.* 5, 2053–2063, e221.
- Whitelam, S., Bretschneider, T., Burroughs, N., 2009. Transformation from spots to waves in a model of actin pattern formation. *Phys. Rev. Lett.* 102, 198103.
- Wu, M., Wu, X., De Camilli, P., 2013. Calcium oscillations-coupled conversion of actin travelling waves to standing oscillations. *Proc. Natl. Acad. Sci. USA* 110, 1339–1344.
- Xiong, Y., Huang, C., Iglesias, P., Devreotes, P., 2010. Cells navigate with a local-excitation, global-inhibition-biased excitable network. *Proc. Natl. Acad. Sci. USA* 107, 17079–17086.
- Xu, J., Wang, F., Van Keymeulen, A., Herzmark, P., Straight, A., Kelly, K., Takuwa, Y., Sugimoto, N., Mitchison, T., Bourne, H., 2003. Divergent signals and cytoskeletal assemblies regulate self-organizing polarity in neutrophils. *Cell* 114, 201–214.
- Yang, L., Dolnik, M., Zhabotinsky, A., Epstein, I., 2002. Pattern formation arising from interactions between turing and wave instabilities. *J. Chem. Phys.* 117, 7259–7265.
- Yizhaq, H., Gilad, E., Meron, E., 2005. Banded vegetation: biological productivity and resilience. *Phys. A: Stat. Mech. Appl.* 356, 139–144.